MULTI-SCALE METHODS FOR MULTI-COMPONENT GRANULAR MATERIALS

ANTHONY R. THORNTON[1,2], THOMAS WEINHART[1], VITALIY OGARKO[1], STEFAN LUDING[1]

[1] *Multi-Scale Mechanics, Department of Mechanical Engineering, University of Twente,
7500 AE Enschede, The Netherlands*
[2] *Mathematics of Computational Science, Department of Applied Mathematics, University of Twente,
7500 AE Enschede, The Netherlands*
Corresponding author: a.r.thornton@utwente.nl

Abstract

In this paper we review recent progress made to understand granular chutes flow using multi-scale modeling techniques. We introduce the discrete particle method (DPM) and explain how to construct continuum fields from discrete data in a way that is consistent with the macroscopic concept of mass and momentum conservation. We present a novel advanced contact detection method that is able of dealing with multiple distinct granular components with sizes ranging over orders of magnitude. We discuss how such advanced DPM simulations can be used to obtain closure relations for continuum frameworks (the mapping between the micro-scale and macro-scale variables and functions): the micro-macro transition. This enables the development of continuum models that contain information about the micro-structure of the granular materials without the need for a priori assumptions.

The micro-macro transition will be illustrated with two granular chute/avalanche flow problems. The first is a shallow granular chute flow where the main unknown in the continuum models is the macro-friction coefficient at the base. We investigate how this depends on both the properties of the flow particles and the surface over which the flow is taking place. The second problem is that of gravity-driven segregation in poly-dispersed granular chute flows. In both these problems we consider small steady-state periodic box DPM simulations to obtain the closure relations.

Finally, we discuss the issue of the validity of such closure-relations for complex dynamic problems, that are a long way from the simple period box situation from which they were obtained. For simple situations the pre-computed closure relations will hold. In more complicated situations new strategies are required were macro-continuum and discrete micro-models are coupled with dynamic, two-way feedback between them.

Key words: coupled multiscale model, multi-component granular materials, Navier-Stokes equation, discrete particle simulations

1. INTRODUCTION

Granular materials are everywhere in nature and many industrial processes use materials in granular form, as they are easy to produce, process, transport and store. Many natural flows are comprised of granular materials and common examples include rock slides than can contain many cubic kilometers of material. Granular materials are, after water, the second most widely manipulated substance on the planet (de Gennes, 2008); however, the field is considerable behind the field of fluids and currently no unified continuum description exists, *i.e.* there is no granular Navier-Stokes style constitutive equations. However, simplified descriptions do exist for certain limiting scenarios: examples include rapid granular flows where kinetic theory is valid (e.g., Jenkins & Savage, 1983; Lun et al., 1984) and shallow dense flows where shallow-layer models are applicable

(e.g. Savage & Hutter, 1989; Gray, 2003; Bokhove & Thornton, 2012). For the case of quasi-static materials the situations is even more complicated and, here, more research on a continuum description is required.

Flows in both nature and industry show highly complex behaviour as they are influenced by many factors such as: poly-dispersity, in size and density; variations in density; nonuniform shape; complex basal topography; surface contact properties; coexistence of static, steady and accelerating material; and, flow obstacles and constrictions.

Discrete particle methods (DPMs) are a very powerful computational tool that allows the simulation of individual particles with complex interactions, arbitrary shapes, in arbitrary geometries, by solving Newton's laws of motion for each particle (e.g. Weinhart et al., 1012). How to capture these elaborate interactions of sintering, complex (nonspherical) shape, breaking and cohesional particles, by the contact model, is an active area of research and many steps forward have recently been made. DPM is very powerful and flexibility tool; however, it is computationally very expensive. With the recent increase in computational power it is now possible to simulate flows containing a few million particles; however, for 1 mm particles this would represent a flow of approximately 1 litre which is many orders of magnitude smaller than the flows found in industrial and natural flows.

Continuum methods are able to simulate the volume of real industrial or geophysical flows, but have to make averaging approximations reducing the properties of a huge number of particles to a handful of averaged quantities. Once these averaged parameters have been tuned via experimental or historical data, these models can be surprisingly accurate; but, a model tuned for one flow configuration often has no prediction power for another setup. Therefore, it is not possible in this fashion to create a unified model capable of describing a new scenario.

DPM can be used to obtain the mapping between the microscopic and macroscopic parameters allowing determination of the macroscopic data without the need for a priori knowledge. In simple situations, it is possible to pre-compute the relations between the particle and continuum (micro-macro transition method); but, in more complicated situations two-way coupled multi-scale modelling (CMSM) is required.

For the micro-macro transition, discrete particle simulations are used to determine unknown functions or parameters in the continuum model as a function of microscopic particle parameters and other state variables; these mappings are referred to as closure relations (e.g. Thornton et al., 2012; 2013). For CMSM, continuum and micro-scale models are dynamically coupled with two-way feedback between the computational models. The coupling is done in selective regions in space and time, thus reducing computational expense and allowing simulation of complex granular flows. For problems
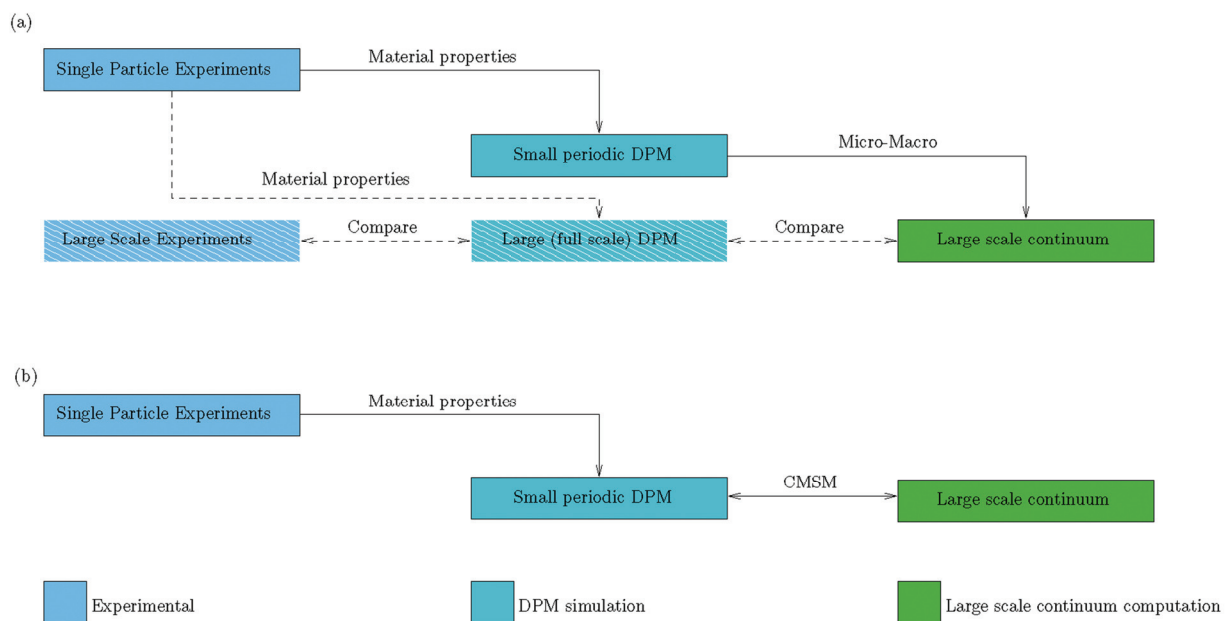

Fig. 1. *Illustration of the modeling philosophy for the undertaken research. Solid lines indicate the main steps of the method and dashed lines the verification steps; (a) shows the idea for the micro-macro transition and (b) for two way coupled multi-scale modelling (CMSM).*

that contain only small complex regions, one can use a localised hybrid approach where a particle method is applied in the complex region and is coupled through the boundary conditions to a continuum solver (Markesteijn, 2011). For large complex regions or globally complex problems, and iterative approach can be used, where a continuum solver is used everywhere, and small particle simulations are run each time the closure relations need to be evaluated, see e.g. (Weinan, 2007).

The ultimate aim of this research would be to determine the unknowns (material/contact properties) in the contact law from a few standard experiments on individual particles.

Our approach is illustrated in figure 1. The idea is to obtain the particle material properties from small (individual) particle experiments and use this information to determine the parameters of the contact model for DPM simulations. We then perform small scale periodic box particles simulations and use this data to determine unknowns in the continuum models (i.e to close the model). It is then expected that this closed continuum model is able to simulate the flow of the same particles in more complex and larger systems. The validity of this closed model will be investigated by comparing its results with both computationally expensive large-scale simulations and experiments. For situations were this one-way coupled micro-macro approach fails, we will use the computationally more expensive two-way coupled models to simulate the flow.

1.1. Outline

It is possible to apply CMSM or micro-macro methods to completely general three-dimensional Cauchy mass and momentum equations and use the DPM to determine the unspecified constitutive relations for the stresses; however, we will not take this approach. We will focus on scenarios where simplifying approximations are made which lead to continuum models (still containing undetermined quantities) that are valid only in certain limits.

In this paper we discuss the approach we are taking, review the current steps we have made and discuss the future directions and open issues with this approach. Firstly, we will consider shallow granular flows (of major importance to many areas of geophysics) and secondly, gravity-driven segregation of poly-dispersed granular material. For the second problem, the efficiency of DPM becomes an issue and a new algorithm will have to be considered.

The outline for the rest of the paper will be: §2 introduction to DPM, §3 how to construct continuum fields from discrete particle data (how to perform the micro-macro transition); §4 the micro-macro transition for shallow granular flows; §5 DPM simulations with wide particle distribution; §5 collision detection; §6 micro-macro transition for segregating flows; and §7 future prospects and conclusions.

2. INTRODUCTION TO DPM

In the discrete particle method, often called the discrete element method, Newton's laws are solved for both the translational and the rotational degrees of freedom. The problem is fully determined by specifying the forces and torques between two interacting particles. Here, we will briefly review three commonly used contact laws for almost spherical granular particles: linear spring-dashpot, Hertzian springs and plastic models.

Each particle i has diameter d_i, mass m_i, position r_i, velocity v_i and angular velocity ω_i. Since we are assuming that particles are almost spherical and only slightly soft, the contacts can be treated as occurring at a single point. The relative distance between two particles i and j is $r_{ij} = |r_i\text{-}r_j|$, the branch vector (the vector from the centre of particle i to the contact point) is $b_{ij} = -\left(d_i - d_{ij}^n\right)\hat{n}/2 = 2$, where the unit normal is $\hat{n}_{ij} = \left(r_i - r_j\right)/r_{ij}$, and the relative velocity is $v_{ij} = v_i\text{-}v_j$, and the overlap is:

$$\delta_{ij}^n = \max\left[0, \frac{1}{2}\left(d_i + d_j\right) - r_{ij}\right]$$

Two particles are in contact if their overlap is positive. The normal and tangential relative velocities at the contact point are given by:

$$v_{ij}^n = \left(v_{ij} \cdot \hat{n}_{ij}\right)\hat{n}_{ij}$$

$$v_{ij}^t = v_{ij} - \left(v_{ij} \cdot \hat{n}_{ij}\right)\hat{n}_{ij} + \omega_i \times b_{ij} - \omega_j \times b_{ji}$$

The total force on particle i is a combination of the normal and tangential contact forces $f_{ij}^n + f_{ij}^t$ from each particle j that is in contact with particle i, and external forces, which for this investigation will be limited to gravity, $m_i g$. Different contact models exist for the normal, f_{ij}^n, and tangential, f_{ij}^t, forces. For each contact model, when the tangential-to-normal force ratio becomes larger than a contact friction coefficient, μ_c, the tangential force yields

and the particles slide, and we truncate the magnitude of the tangential force as necessary to satisfy $\left|\boldsymbol{f}_{ij}^{t}\right| \leq \mu^{c}\left|\boldsymbol{f}_{ij}^{n}\right|$. We integrate the resulting force and torque relations in time using Velocity-Verlet and forward Euler (Allen & Tildesley, 1989) with a time step $\Delta_{t} = t_{c} = 50$, where t_{c} is the collision time, see e.g. (Luding, 2008):

$$t_{c} = \frac{\pi}{\sqrt{\dfrac{k^{n}}{m_{ij}} - \left(\dfrac{\gamma^{n}}{2m_{ij}}\right)^{2}}} \tag{1}$$

with the reduced mass $m_{ij} = m_i m_j/(m_i + m_j)$.

For the spring-dashpot case (Cundall & Strack, 1979; Luding, 2008; Weinhart, 2012a) the normal, $\boldsymbol{f}_{ij(sd)}^{n}$, and tangential, $\boldsymbol{f}_{ij(sd)}^{t}$, forces are modelled with linear elastic and linear dissipative contributions, hence:

$$\boldsymbol{f}_{ij(sd)}^{n} = k^{n}\delta_{ij}^{n}\hat{\boldsymbol{n}}_{ij} - \gamma^{n}\boldsymbol{v}_{ij}^{n}, \quad \boldsymbol{f}_{ij(sd)}^{t} = -k^{t}\delta_{ij}^{t} - \gamma^{t}\boldsymbol{v}_{ij}^{t} \tag{2}$$

with spring constants k^n, k^t and damping coefficients γ^n, γ^t. The elastic tangential displacement, $\boldsymbol{\delta}_{ij}^{t}$, is defined to be zero at the initial time of contact, and its rate of change is given by:

$$\frac{d}{dt}\boldsymbol{\delta}_{ij}^{t} = \boldsymbol{v}_{ij}^{t} - r_{ij}^{-1}\left(\boldsymbol{\delta}_{ij}^{t} \cdot \boldsymbol{v}_{ij}\right)\boldsymbol{n}_{ij} \tag{3}$$

In equation (3), the first term is the relative tangential velocity at the contact point, and the second term ensures that $\boldsymbol{\delta}_{ij}^{t}$ remains normal to $\boldsymbol{n}_{ij}$, see (Weinhart, 2012a) for details. This model is designed to model particles that are elastic, but dissipated with clearly defined coefficient of restitution, ε.

For the Hertzian case we modify the interaction force with:

$$\boldsymbol{f}_{ij(Hertz)}^{n/t} = \sqrt{\frac{\delta_{ij}^{n}}{d}}\,\boldsymbol{f}_{ij(sd)}^{n/t} \tag{4}$$

see e.g. (Silbert et al., 2001). This models follows from the theory of elasticity and takes account of the full non-linear elastic response.

Finally, for the plastic case (designed to capture small plastic deformation) we modify the normal force using the (hysteretic) elastic-plastic form of Walton and Braun e.g. (Luding, 2008; Walton & Braun, 1986), therefore, in the normal direction a different spring constant is taken for loading and unloading/reloading of the contact and no dash-pot is used i.e.:

$$\boldsymbol{f}_{ij(p)}^{n} = \begin{cases} k_{1}^{n}\delta_{ij}^{n}\hat{\boldsymbol{n}}_{ij} & \text{if} & k_{2}^{n}\delta_{ij}^{e} \geq k_{1}^{n}\delta_{ij}^{n} \\ k_{2}^{n}\delta_{ij}^{e}\hat{\boldsymbol{n}}_{ij} & \text{if} & k_{1}^{n}\delta_{ij}^{n} \geq k_{2}^{n}\delta_{ij}^{e} > 0 \\ 0 & \text{if} & k_{2}^{n}\delta_{ij}^{e} \leq 0 \end{cases} \tag{5a}$$

$$\boldsymbol{f}_{ij(p)}^{t} = \boldsymbol{f}_{ij(sd)}^{t} = -k^{t}\boldsymbol{\delta}_{ij}^{t} - \gamma^{t}\boldsymbol{v}_{ij}^{t} \tag{5b}$$

with $\delta_{ij}^{e} = \delta_{ij}^{n} - \delta_{ij}^{\max}\left(1 - k_{1}^{n}/k_{2}^{n}\right)$ and, $\delta_{ij}^{\max} = \max \delta_{ij}^{n}$ is the maximum overlap during the contact. Unlike (Luding, 2008, Walton & Braun, 1986), we take k_{2}^{n} to be constant, so that the normal coefficient of restitution is given by $\varepsilon_{n} = \sqrt{k_{1}^{n}/k_{2}^{n}}$. However, for enduring contacts the dissipation is smaller than in the spring-dashpot case, since oscillations on the unloading/reloading (k_{2}^{n}) branch do not dissipate energy. For a more detailed review of contact laws, in general, we refer the reader to (Luding, 2008).

3. THE MICRO-MACRO TRANSITION

For all multi-scale methods, one of the biggest challenges is how to obtain continuum fields from large amounts of discrete particle data. Here, we give a short overview, then review in more detail the approach we prefer.

There are many papers in the literature on how to go from the discrete to the continuum: binning micro-scale fields into small volumes (Irving & Kirkwood, 1950; Schoeld & Henderson, 1982; Luding, 2004; Luding et al., 2001), averaging along planes (Todd et al., 1995), or coarse-graining spatially and temporally (Babic, 1997; Shen & Atluri, 2004; Goldhirsch, 2010). Here, we use the coarse graining approach described by Weinhart et al. (2012b) as this is still valid within one coarse-graining width of the boundary.

The coarse-graining method has the following advantages over other methods: (i) the fields produced automatically satisfy the equations of continuum mechanics, even near the flow base; (ii) it is neither assumed that the particles are rigid nor spherical; and, (iii) the results are even valid for single particles as no averaging over groups of particles is required. The only assumptions are that each particle pair has a single point of contact (i.e., the particle shapes are convex), the contact area can be

replaced by a contact point (i.e., the particles are not too soft), and that collisions are not instantaneous.

3.1. Notation and basic ideas

Vectorial and tensorial components are denoted by Greek letters in order to distinguish them from the Latin particle indices i; j. Bold vector notation will be used when convenient.

Assume a system given by N_f owing particles and N_b fixed basal particles with $N = N_f + N_b$. Since we are interested in the flow, we will calculate macroscopic fields pertaining to the owing particles only. From statistical mechanics, the microscopic mass density of the flow, ρ^{mic}, at a point r at time t is defined by:

$$\rho^{mic}(r,t) = \sum_{i=1}^{N_f} m_i \delta \left[r - r_i(t) \right] \qquad (6)$$

where $\delta(r)$ is the Dirac delta function and m_i is the mass of particle i. The following definition of the macroscopic density of the flow is used:

$$\rho(r,t) = \sum_{i=1}^{N_f} m_i W \left[r - r_i(t) \right] \qquad (7)$$

thus replacing the Dirac delta function in (6) by an integrable 'coarse-graining' function w whose integral over space is unity. We will take the coarse-graining function to be a Gaussian:

$$W\left(r - r_i(t) \right) = \frac{1}{\left(\sqrt{2\pi} w \right)^3} \exp\left(-\frac{\left| r - r_i(t) \right|^2}{2w^2} \right) \qquad (8)$$

with width or variance w. Other choices of the coarse-graining function are possible, but the Gaussian has the advantage that it produces smooth fields and the required integrals can be analysed exactly. According to Goldhirsch (2010), the coarse-grained fields depend only weakly on the choice of function, and the width w is the key parameter.

It is clear that as $w \rightarrow 0$ the macroscopic density defined in (8) reduces to the one in (7). The coarse-graining function can also be seen as a convolution integral between the micro and macro definitions, i.e.:

$$\rho(r,t) = \int_{R^3} W\left(r - r_i(t) \right) \rho^{mic}(r',t) dr' \qquad (9)$$

3.2. Mass balance

Next, we will consider how to obtain the other fields of interest: the momentum density vector and the stress tensor. As before, all macroscopic variables will be defined in a way compatible with the continuum conservation laws.

The coarse-grained momentum density vector $p(r, t)$ is defined by:

$$p_\alpha(r,t) = \sum_{i=1}^{N_f} m_i v_{i\alpha}(t) W\left(r - r_i \right) \qquad (10)$$

where the $v_{i\alpha}$'s are the velocity components of particle i. The macroscopic velocity field $V(r,t)$ is then defined as the ratio of momentum and density fields,:

$$V_\alpha(r,t) = \frac{p_\alpha(r,t)}{\rho(r,t)} \qquad (11)$$

It is straightforward to confirm that equations (7) and (10) satisfy exactly the continuity equation:

$$\frac{\partial \rho}{\partial t} + \frac{\partial p_\alpha}{\partial r_\alpha} = 0 \qquad (12)$$

with the Einstein summation convention for Greek letters.

3.3. Momentum balance

Finally, we will consider the momentum conservation equation with the aim of establishing the macroscopic stress field. In general, the desired momentum balance equations are written as:

$$\frac{\partial p_\alpha}{\partial r_\alpha} = -\frac{\partial}{\partial r_\beta}\left[\rho V_\alpha V_\beta \right] + \frac{\partial \sigma_{\alpha\beta}}{\partial r_\beta} + t_\alpha + \rho g_\alpha \qquad (13)$$

where $\sigma_{\alpha\beta}$ is the stress tensor, and g_α is the gravitational acceleration vector. Since we want to describe boundary stresses as well as internal stresses, the boundary interaction force density, or surface traction density, t, has been included, as described in detail in (Weinhart et al. 2012b).

Expressions (10) and (11) for the momentum p and the velocity V have already been defined. The next step is to compute their temporal and spatial derivatives, respectively, and reach closure. Then after some algebra, see (Weinhart et al., 2012b) for details, we arrive at the following expression for the stress:

$$\sigma_{\alpha\beta} = -\sum_{i=1}^{N_f}\sum_{j=1+1}^{N_f} f_{ij\alpha} r_{ij\beta} \int_0^1 W\left(\boldsymbol{r}-\boldsymbol{r}_i+s\boldsymbol{b}_{ik}\right)ds$$

$$-\sum_{i=1}^{N_f}\sum_{k=1}^{N_f} f_{ik\alpha}^b b_{ik\beta} \int_0^1 W\left(\boldsymbol{r}-\boldsymbol{r}_i+s\boldsymbol{b}_{ik}\right)ds - \sum_{i=1}^{N_f} m_i v_{i\alpha}^, v_{i\beta}^, W_i$$

(14)

Equation (14) differs from the results of Goldhirsch.(2010) by an additional term that accounts for the stress created by the presence of the base, as detailed by Weinhart et al., (2012b). The contribution to the stress from the interaction of two flow particles i; j is spatially distributed along the contact line from $\boldsymbol{r}_i$ to $\boldsymbol{r}_j$, while the contribution from the interaction of particles i with a fixed particle k is distributed along the line from $\boldsymbol{r}_i$ to the contact point $c_{ik} = \boldsymbol{r}_i + \boldsymbol{b}_{ik}$. There, the boundary interaction force density:

$$t_\alpha = \sum_{i=1}^{N_f}\sum_{k=1}^{N_b} f_{ik\alpha} W\left(\boldsymbol{r}-\boldsymbol{c}_{ik}\right)$$

(15)

is active, measuring the force applied by the base to the flow. It has nonzero values only near the basal surface and can be introduced into continuum models as a boundary condition.

The strength of this method is that the spatially coarse-grained fields by construction satisfy the mass and momentum balance equations exactly at any given time, irrespective of the choice of coarse-graining function. Further details about the accuracy of the stress definition (14) are discussed by Weinhart et al., (2012b). The expression for the energy is also not treated in this publication, we refer the interested reader to (Babic, 1997).

4. SHALLOW GRANULAR FLOWS

4.1. Background

Shallow-layer granular continuum models are often used to simulate geophysical mass flows, including snow avalanches (Cui et al., 2007), dense pyroclastic flows, debris flows (Denlinger & Iverson, 2001), block and ash flows (Dalby et al., 2008), and lahars (Williamset al., 2008). Such shallow-layer models involve approximations reducing the properties of a huge number of individual particles to a handful of averaged quantities. Originally these models were derived from the general continuum incompressible mass and momentum equations, using the long-wave approximation (Savage & Hutter, 1989; Gray, 2003; Bokhove & Thornton, 2012)

for shallow variations in the flow height and basal topography. Despite the massive reduction in degrees of freedom made, shallow-layer models tend to be surprisingly accurate, and are thus an effective tool in modelling geophysical flows. Moreover, they are now used as a geological risk assessment and hazard planning tool (Dalby et al., 2008). In addition to these geological applications, shallow granular equations have been applied to analyse small-scale laboratory chute flows containing obstacles (Gray, 2003), wedges (Hakonardottir & Hogg, 2005; Gray, 2007) and contractions (Vreman, 2007), showing good quantitative agreement between theory and experiment.

We will consider flow down a slope with inclination θ, the x-axis downslope, y-axis across the slope and the z-axis normal to the slope. In general, the free-surface and base locations are given by $z = s(x,y)$ and $z = b(x,y)$, respectively. Here, we will only consider flows over rough at surfaces where b can be taken as constant. The height of the flow is $h = s - b$ and velocity components are $\boldsymbol{u} = (u,v,w)^T$. Depth-averaging the mass and momentum balance equations and retaining only leading and first order terms (in the ratio of height to length of the flow) yields the depth-averaged shallow-granular equations, (e.g.Gray, 2003), which in one-dimension are given by:

$$\frac{\partial h}{\partial t} + \frac{\partial}{\partial x}\left(h\bar{u}\right) + \frac{\partial}{\partial y}\left(h\bar{v}\right) = 0$$

(16a)

$$\frac{\partial}{\partial t}\left(h\bar{u}\right) + \frac{\partial}{\partial x}\left(\alpha h\bar{u}^2 + K\frac{g}{2}h^2\cos\theta\right) = S_x$$

(16b)

where g is the gravitational acceleration, $\bar{u}$ the depth-averaged velocity and the source term is given by:

$$S_x = gh\cos\theta\left(\tan\theta - \mu\frac{\bar{u}}{\sqrt{\bar{u}^2+\bar{v}^2}}\right)$$

Before these equations can be solved, closure relations need to be specified for three unknowns: the velocity shape factor, α, the ratio of the two diagonal stress components, K, and the friction, μ, between the granular materials and the basal surface over which it flows.

These closure relations can either be postulated (from theory or phenomenologically), or determined from experiments or DPM simulations. Our philosophy was to determine these unknown relations using

small-scale periodic box simulations DPMs similar to the ones used by Silbert et al. (2001).

Below some of the main findings are summarized. Initially, we consider only the springdashpot contact model and looked at the closures across different basal surfaces (Weinhart et al., 2012a). The chute is periodic and of size $20d \times 10d$ in the $x \times y$-directions, with inclination θ, see figure 2. In this case flow particles are monodispersed. The base was created from particles and roughness was changed by modifying the ratio of the size of base and flow particles, λ.

4.2. Closure for K

For the shallow layer theory presented in (16), K, is the ratio of two stress component $K = \sigma_{xx}/\sigma_{zz}$. First the K was found to be linear in the inclination angle and independent of λ (for all but the smooth base case of $\lambda = 0$):

$$K^{fit} = 1 + \frac{\theta - d_1}{d_0} \qquad (17)$$

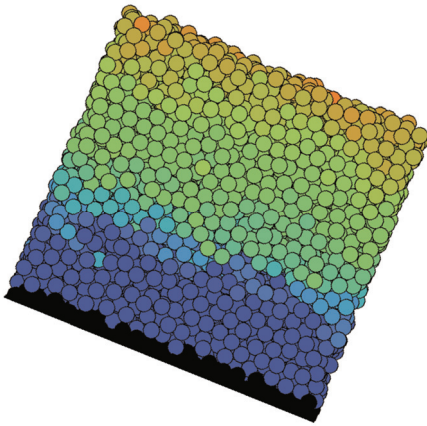with $d_0 = 132^o$ and $d_1 = 21.30^o$.

Fig. 2. *DPM simulation for $N_f/200 = 17:5$, inclination $\theta = 24$ and the diameter ratio of free and fixed particles, $\lambda = 1$, at time $t = 2000$; gravity direction g as indicated. The domain is periodic in x- and y-directions. In the z-direction, fixed particles (black) form a rough base while the surface is unconstrained. Colours indicate speed: increasing from blue via green to orange.*

4.3. Closure for μ

By far the most studies closure relation for shallow granular flows is the basal friction coefficient μ. In the early models a constant friction coefficient was assumed (Hungr & Morgenstern, 1984; Savage & Hutter, 1989), i.e. $\mu = \tan \delta$, where δ is a fixed basal frictional angle. For these models, steady uni-

form flow is only possible at a single inclination, δ, below which the flow arrests, and above which the flow accelerates indefinitely. Detailed experimental investigations (GDR MiDi, 2004; Pouliquen, 1999; Pouliquen & Forterre, 2002) for the flow over rough uniform beds showed that steady flow emerges at a range of inclinations, $\theta_1 < \theta < \theta_2$, where θ_1 is the minimum angle required for flow, and θ_2 is the maximum angle at which steady uniform flow is possible. In (Pouliquen & Forterre, 2002), the measured height $h_{stop}(\theta)$ of stationary material left behind when a owing layer has been brought to rest, was fitted to:

$$\frac{h_{stop}(\theta)}{Ad} = \frac{\tan(\theta_2) - \tan(\theta)}{\tan(\theta) - \tan(\theta_1)} \quad \theta_1 < \theta < \theta_2 \qquad (18)$$

where d is the particle diameter and A a characteristic dimensionless scale over which the friction varies. They also observed that the Froude number $F = u/\sqrt{gh\cos(\theta)}$, scaled linear with this curve:

$$F = \frac{\beta h}{h_{stop}(\theta)} - \gamma \quad \theta_1 < \theta < \theta_2 \qquad (19)$$

where β and γ are two experimentally determined constants. From these relations you can show that the friction closure is given by:

$$\mu(h, F) = \tan(\theta_1) + \frac{\tan(\theta_2) - \tan(\theta_1)}{\dfrac{\beta h}{Ad(F + \gamma)} + 1} \qquad (20)$$

This experimentally determined law has previously been shown to hold from DPM simulations (e.g. Silbert et al., 2001). In (Thornton, 2012; Weinhart et al., 2012a) we investigate how the parameters A, θ_1, θ_2, and γ change as a function of the contact friction between bed and owing particles, the particle size ratio λ and even the type of contact law. The main conclusion were:

–   The law (18) holds for the spring-dashpot, plastic and Hertzian contact models
–   The properties of the basal particles have very little affect on the macroscopic friction, that is, only a weak effect on and.
–   The geometric roughness λ is more important than the contract friction in the interaction law, μ_c.
–   The coefficient of restitution of the particles only affects, not the friction angles.

Full details of the values of A, θ_1, θ_2, and γ as a function of both macro- and microscopic parameters can be found in (Thornton, 2012; Weinhart et al., 2012a).

This was done in two steps: firstly, it was observed that the vertical flow velocity structure contained three parts, see figure 4 for details. These were then fitted separately and from these fits the
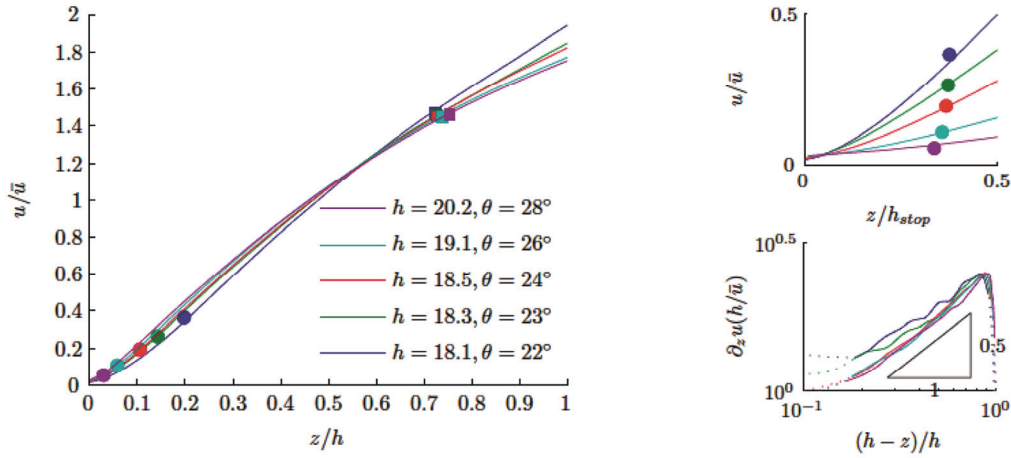

Fig. 3. *Flow velocity profiles for varying height for 4000 particles and $\lambda = 1$. We observe a Bagnold velocity profile,*

$$u = \frac{5}{3}\bar{u}\left[1 - \left(\frac{h-z}{h}\right)^{3/2}\right],$$ *in the bulk, a linear profile near the surface and a convex profile near the base $[z < b_1 h_{stop}(\theta)/h]$ with $b_1 = 9.42$.*

4.4. Closure for α

Finally, we consider the closure the velocity shape factor. This is the shape of the velocity profile with height and is defined as

$$\alpha = \frac{1}{h}\frac{\int_b^s u^2 dz}{\int_b^s u\,dz} \qquad (21)$$

shape factor α was computed. The values of α as a function of height and angle, θ, is shown in figure 4.

4.5. Future directions

We have now established closure relations for shallow-granular flows and the natural question of the range of validity of closure relations derived from this small steady periodic box simulations. This closed continuum model has recently been implemented in an in-house discontinuous Galerkin finite element package, hpGEM (Pesch, 2007; van der Vegt). A series of test cases and currently being investigated include complicated features with contractions and obstacles. The results of this closed model are compared with computationally expensive full-scale DPM simulations of the same scenarios. This comparison and verification set is represented by the dashed lines in figure 1.

It is anticipated that this closured continuum model will work fine for simple flow scenarios; however, for complex flow containing particle free regions and static mate-
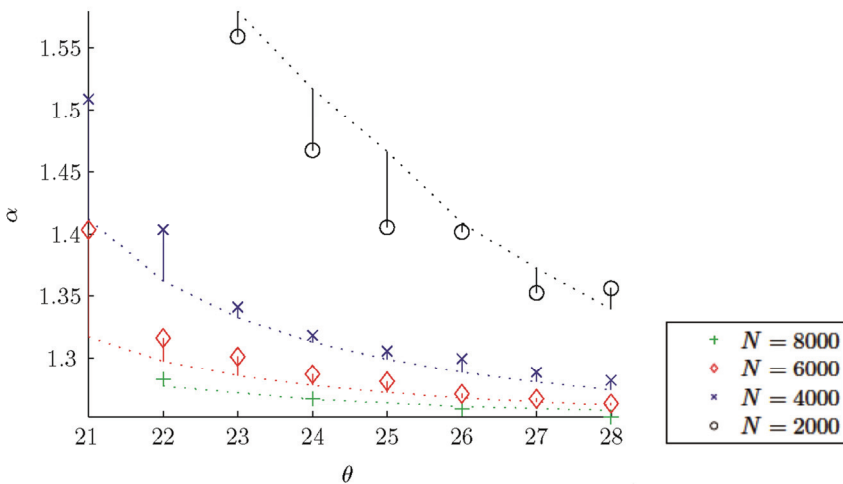

Fig. 4. *Shape factor α from simulations (markers), for case $\lambda = 1$, and fit $\alpha(h,\theta)$ (dotted lines). For comparison, plug flow $\alpha = 1$, Bagnold profile $\alpha = 1:25$ and lines profile $\alpha = 1:5$.*

rials it is likely to fail. For this situation, a fully two-way coupled code will have to be developed. More discussion of problems associated with the development of this code can be found in chapter 7.

5. COLLISION DETECTION

The performance of the DPM computation relies on several factors, which include both the contact model and the contact detection algorithm. The collision detection of short-range pair wise interactions between particles in DPM is usually one of the most time-consuming tasks in computations (Williams & O'Connor, 1999). If you were to undertake the task of collision detection in a naive fashion you would have to perform N^2 checks were N is the number of particles; however, this becomes impractical even for relatively small systems.

The most commonly used method for contact detection of nearly mono-sized particles with short-range forces is the Linked-Cell method (Hockney & Eastwood, 1981; Allen & Tildesley, 1989). Due to its simplicity and high performance, it has been utilized since the beginning of particle simulations, and is easily implemented in parallel codes (Form, 1993; Stadler et al., 1997).

Nevertheless, the Linked-Cell method is unable to efficiently deal with particles of greatly varying sizes (Iwai, 1999), which will be the case in the next problem considered. This can effectively be addressed by the use of a multilevel contact detection algorithm (Ogarko & Luding, 2012), which we review here. This advanced contact detection algorithm is already implemented in Mercury (Thornton et al.), the open-source code developed here, and that is used for all the simulations in this paper. An extensive review of various approaches to contact detection is given in Munjiza, 2004. The performance difference between them is studied in (Muth, 2007; Ogarko & Luding, 2012; Raschdorf & Kolonko, 2011).

5.1. Algorithm

The present algorithm is designed to determine all the pairs in a set of N spherical particles in a d-dimensional Euclidean space that overlap. Every particle is characterized by the position of its centre r_p and its radius a_p. For differently-sized spheres, a_{min} and a_{max} denote the minimum and the maximum particle radius, respectively, and $\sigma = a_{min}/a_{max}$ is the extreme size ratio.

The algorithm is made up of two phases. In the first 'mapping phase' all the particles are mapped into a hierarchical grid space (subsection 5.1.1). In the second 'contact detection phase' (subsection 5.1.2) for every particle in the system the potential contact partners are determined, and the geometrical intersection tests with them are made.

5.1.1. Mapping phase

The d-dimensional hierarchical grid is a set of L regular grids with different cell sizes. Every regular grid is associated with a hierarchy level $h \in 1, 2, \ldots, L$, where L is the integer number of hierarchy levels. Each level h has a different cell size $s_h \in R$, where the cells are d-dimensional cubes. Grids are ordered with increasing cell size so that $h = 1$ corresponds to the grid with smallest cell size, i.e., $s_h < s_h + 1$. For a given number of levels and cell sizes, the hierarchical grid cells are defined by the following spatial mapping, M, of points $r \in R^d$ to a cell at specified level h:

$$M : (\boldsymbol{r}, h) \to \boldsymbol{c} = \left(\left[\frac{r_1}{s_h} \right], \ldots, \left[\frac{r_d}{s_h} \right] \right) \qquad (22)$$

where $[r]$ denotes the floor function (the largest integer nor greater than r). The first d components of $a(d + 1)$-dimensional vector c represent cell indices (integers), and the last one is the associated level of hierarchy. The latter is limited whereas the former are not.

It must be noted that the cell size of each level can be set independently, in contrast to contact detection methods which use a tree structure for partitioning the domain (Ericson, 1993; Raschdorf & Kolonko, 2011; Thatcher, 2000) where the cell sizes are taken as double the size of the previous lower level of hierarchy, hence $s_h + 1 = 2s_h$. The flexibility of independent s_h allows one to select the optimal cell sizes, according to the particle size distribution, to improve the performance of the simulations. How to do this is explained by (Ogarko & Luding, 2012).

Using the mapping M, every particle p can be mapped to its cell:

$$c_p = M \left[r_p, h(p) \right] \qquad (23)$$

where $h(p)$ is the level of insertion to which particle p is mapped to. The level of insertion $h(p)$ is the lowest level where the cell is big enough to contain the particle p:

$$h(p)c_p = \left\{ \min_{1 \leq h \leq L} h : s_h \geq 2r_p \right\} \qquad (24)$$

In this way the diameter of particle p is smaller or equal to the cell size in the level of insertion and therefore the classical Linked-Cell method (Allen & Tildesley, 1989) can be used to detect the contacts among particles within the same level of hierarchy.

Figure 5 illustrates a 2-dimensional two-level grid for the special case of a bi-disperse system with $a_{min} = 3/2$, size ratio $\sigma = 8/3$, and cell sizes $s_1 = 3$, and $s_2 = 8$. Since the system contains particles of only two different sizes, two hierarchy levels are sufficient here.
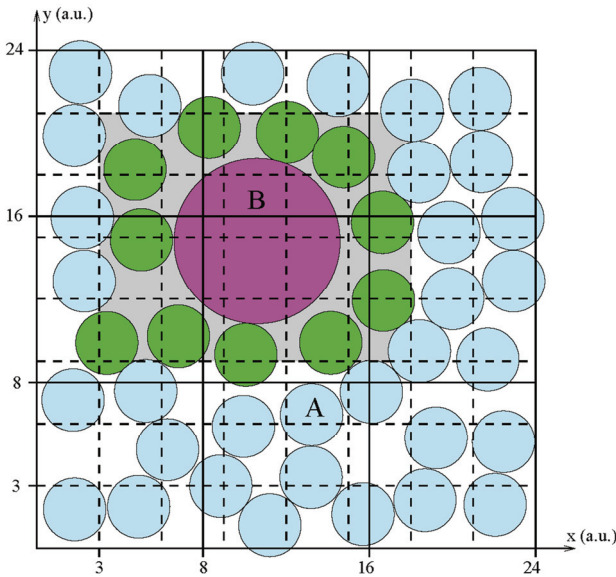

Fig. 5. *A 2-dimensional two-level grid for the special case of a bi-disperse system with cell sizes $s_1 = 2a_{min} = 3$, and $s_2 = 2a_{max} = 8$ (a.u.). The first level grid is plotted with dashed lines while the second level is plotted with solid lines. The radius of the particle B is $a_B = 4$ (a.u.) and its position is $r_B = (10.3; 14.4)$. Therefore, according to equations (23) and (24), particle B is mapped to the second level to the cell $c_B = (1, 1, 2)$. Correspondingly, particle A is mapped to the cell $c_A = (4, 2, 1)$. The cells where the cross-level search for particle B has to be performed from (1,3,1) to (5,6,1) are marked in grey, and the small particles which are located in those cells are dark (green). Note, that in the method of Iwai et al. (1999) the search region starts at cell (1, 2, 1), i.e., one more layer of cells (which also includes particle A).*

5.1.2. Contact detection phase

The contact detection is split into two steps, and the search is done by looping over all particles p and performing the first and second steps consecutively for each p. The first step is the contact search at the level of insertion of p, $h(p)$, using the classical Linked-Cell method (Allen & Tildesley, 1989). The search is done in the cell where p is mapped to, i.e., c_p, and in its neighbour (surrounding) cells. Only

half of the surrounding cells are searched, to avoid testing the same particle pair twice.

The second step is the cross-level search. For a given particle p, one searches for potential contacts only at levels h lower than the level of insertion: $1 \leq h < h(p)$. This implies that the particle p will be checked only against the smaller ones, thus avoiding double checks for the same pair of particles. The cross-level search for particle p (located at $h(p)$) with level h is detailed here:

1. Define the cells c^{start} and c^{end} at level h as

$$c^{start} := M(r_c^-, h), \text{ and } c^{end} := M(r_c^+, h) \qquad (25)$$

where a search box (cube in 3D) is defined by $r_c^{\pm} = r_p \pm \alpha \sum_{i=1}^{d} e_i$, with $\alpha = a_p + 0.5s_h$ and e_i is the standard basis for R^d. Any particle q from level h, i.e., $h(q) = h$, with centre x_q outside this box can not be in contact with p, since the diameter of the largest particle at this level can not exceed s_h.

2. The search for potential contacts is performed in every cell $c = (c_1, \ldots , c_d; h)$ for which

$$c_i^{start} \leq c_i \leq c_i^{end} \text{ for all } i \in [1, d],$$
$$\text{and } c_{d+1} = h < h(p) \qquad (26)$$

where c_i denotes the i-th component of vector c. In other words, each particle which was mapped to one of these neighbour cells is tested for contact with particle p. In figure 5, the level $h = 1$ cells where that search has to be performed (for particle B) are marked in grey.

To test two particles for contacts, first, the axis-aligned bounding boxes (AABB) of the particles (Moore & Wilhelms, 1988) are tested for overlap. Then, for every particle pair which passed this test, the exact geometrical intersection test is applied (Particles p and q collide only if $\|r_p - r_q\| < a_p + a_q$, where $\|\cdot\|$ is Euclidean norm.). Since the overlap test for AABBs is computationally cheaper than for spheres, performing such test first usually increases the performance.

5.2. Performance test

In this section we present numerical results on the performance of the algorithm when applied for bi-disperse particle systems, i.e., two different sizes, as will be considered for the segregation case in the next section. For such systems, the cell sizes of the two-level grid can be easily selected as the two diameters of each particle species. However, for some

situations this may be not as efficient as the use of the single-level Linked-Cell method, as we show below. How the algorithm performs for poly-disperse systems and how to select optimal cell sizes and number of levels for such systems is shown in (Ogarko & Luding, 2012).

We use homogeneous and isotropic disordered systems of colliding elastic spherical particles in a unit cubical box with hard walls. The motion of particles is governed by Newton's second law with a linear elastic contact force during overlap. For simplicity, every particle undergoes only translational motion (without rotation) and gravity is set to zero. For more details on numerical procedure and preparation of initial configurations see (Ogarko & Luding, 2012).

We consider a bi-disperse size distribution with the same volume of small and large particles. This distribution can be characterized by only one parameter, σ, which is the ratio between small and large particle radius, i.e., in this convention $0 < \sigma \leq 1$. The considered systems have volume fraction close to the jamming density. Namely, the volume fraction of systems with $\sigma = 0.9, 0.8, 0.7, 0.6, 0.5, 0.4, 0.3, 0.2$ is $\nu \approx 0.631, 0.635, 0.642, 0.652, 0.665, 0.682, 0.703, 0.723$, respectively. For the influence of the volume fraction on the performance of the algorithm, see (Ogarko & Luding, 2011).
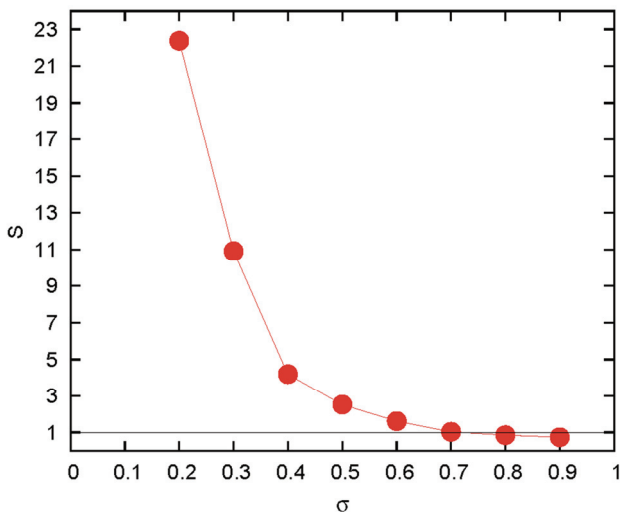

Fig. 6. *The speed-up S of the two-level grid relative to the single-level grid (Linked-Cell method) for bidisperse systems with different size ratios σ. The number of particles used is N = 128 000 for σ > 0.4, N = 256 000 for σ = 0.3 and N = 768 000 for σ = 0.2. Three independent runs were performed for every σ and the average CPU time values are used for the calculation of S.*

Figure 6 shows the speed-up S of the two-level grid relative to the single-level grid (Linked-Cell method). For similar sizes of particles, i.e., $\sigma > 0.7$,

the use of the two-level grid slightly (within 40%) slows down the performance of the algorithm. This is due to the overhead associated with cross-level tests. With increasing difference in particle size, i.e., decreasing σ, the speed-up is increasing. For $\sigma > 0.7$ the speed-up exceeds unity and the use of the two-level grid becomes advantageous. The maximum speed-up of 22 is achieved in the case of the lowest considered $\sigma = 0.2$. Much higher speed-up is expected for $\sigma < 0.2$.

6. MICRO-MACRO FOR SEGREGATING FLOWS

6.1. Background

Except for the very special case of all particles being identical in density and size, segregation effects can be observed in granular materials. In both natural and industrial situations, segregation plays an important, but poorly understood, role on the flow dynamics Iverson, 2003; Shinbrot et al, 1999). There are many mechanisms for the segregation of dissimilar grains in granular flows; however, segregation due to size-differences is often the most important (Drahun & Bridgewater, 1983). We will focus on dense granular chute flows where kinetic sieving (Middleton, 1970; Savage & Lun, 1988) is the dominant mechanism for particle-size segregation. The basic idea is: as the grains avalanche down-slope, the local void ratio fluctuates and small particles preferentially fall into the gaps that open up beneath them, as they are more likely to fit into the available space than the large ones. The small particles, therefore, migrate towards the bottom of the flow and lever the large particles upwards due to force imbalances. This was termed squeeze expulsion by Savage and Lun (1988).

The first model of kinetic sieving was developed by Savage and Lun (1988), using a statistical argument about the distribution of void spaces. Later, Gray and Thornton (2005) developed a similar model from a mixture-theory framework. Their derivation has two key assumptions: firstly, as the different particles percolate past each other there is a Darcy-style drag between the different constituents (i.e., the small and large particles) and, secondly, particles falling into void spaces do not support any of the bed weight. Since the number of voids available for small particles to fall into is greater than for large particles, it follows that a higher percentage of the small particles will be falling and, hence, not sup-

porting any of the bed load. In recent years, this segregation theory has been developed and extended in many directions: including the addition of a passive background fluid (Thornton et al., 2006) the effect of diffusive remixing (Gray & Chugunov, 2006), and the generalization to multi-component granular flows (Gray & Ancey, 2011). We will use the two-particle size segregation-remixing version derived by Gray and Chugunov (2006); however, it should be noted that Dolgunin and Ukolov (1995) were the first to suggest this form, by using phenomenological arguments. The bi-dispersed segregation remixing model contains two dimensionless parameters. These in general will depend on flow and particle properties, such as: size-ratio, material properties, shear-rate, slope angle, particle roughness, etc. One of the weaknesses of the model is that it is not able to predict the dependence of the two parameters on the particle and flow properties. Here are summarized the main results of (Thornton, 2013), where the ratio of these parameters was determined from DPM simulations.

The two-particle segregation-remixing equation (Gray & Chugunov, 2006) takes the form of a non-dimensional scalar conservation law for the small particle concentration - as a function of the spatial coordinates $\hat{x}$, $\hat{y}$ and $\hat{z}$, and time $\hat{t}$.

$$\frac{\partial \phi}{\partial \hat{t}} + \frac{\partial}{\partial \hat{x}}(\phi \hat{u}) + \frac{\partial}{\partial \hat{y}}(\phi \hat{v}) + \frac{\partial}{\partial \hat{z}}(\phi \hat{w}) - \\ \cdot \frac{\partial}{\partial \hat{z}}\left[S_r \phi (1-\phi) \right] = \frac{\partial}{\partial \hat{z}}\left(D_r \frac{\partial \phi}{\partial \hat{z}} \right) \quad (27)$$

where S_r is the dimensionless measure of the segregation-rate, whose form in the most general case is discussed in Thornton et al. (2006) and D_r is a dimensionless measure of the diffusive remixing. In (27), ∂ is used to indicate a partial derivative, and the 'hat' a dimensionless variable. $\hat{x}$ is the downslope coordinate, $\hat{y}$ the cross-slope and $\hat{z}$ normal to the base coordinate. Furthermore $\hat{u}$, $\hat{v}$ and $\hat{w}$ are the dimensionless bulk velocity components in the $\hat{x}$, $\hat{y}$ and $\hat{z}$ directions, respectively.

The conservation law (27) is derived under the assumption of uniform porosity and is often solved subject to the condition that there is no normal flux of particles through the base or free surface of the flow.

We limit our attention to small-scale DPM simulations, periodic in the x and y-directions, and investigate the final steady-states. Therefore, we are inter-

ested in a steady state solution to (27) subject to no-normal flux boundary condition, at $\hat{z} = 0$ (the bottom) and 1 (the top), that is independent of $\hat{x}$ and $\hat{y}$. Gray and Chugunov (2006) showed that such a solution takes the form:

$$\phi = \frac{\left[1 - \exp(-\phi_0 P_s)\right] \exp(\phi_0 - z) P_s}{1 - \exp\left[-(1-\phi_0) P_s\right] + \left[1 - \exp(-\phi_0 P_s)\right] \exp(\phi_0 - z) P_s} \quad (28)$$

where $P_s = S_r / D_r$ is the segregation Peclet number and ϕ_0 is the mean concentration of small particles. This solution represents a balance between the last two terms of (27) and is related to the logistic equation. In general, P_s will be a function of the particle properties, and we will use DPM to investigate the dependence of P_s on the particle size ratio $\sigma = d_s/d_l$.

It should be noted that σ has been defined such that it is consistent with the original theory of Savage and Lun (1988); however, with this definition only values between 0 and 1 are possible. Therefore, we will present the results in terms of σ^{-1}, which ranges from 1 to infinity.

6.2. The Micro-Macro transition

Figure 7 shows a series of images from the DPM simulations at different times and values of σ^{-1}. The simulations take place in a box, which is periodic in x and y, is $5d_s$ wide and $83.3d_s$ long, inclined at an angle of 25 to the horizontal. The base was created by adding fixed small particles randomly to a flat surface. The simulations are performed with 5000 flowing small particles and the number of large particles is chosen such that the total volume of large and small particles is equal, i.e., $\phi_0 = 0:5$ (to within the volume of one large particle).

Figure 8 shows a fit of equation (28) to the small particle volume fraction for several cases. The fit is performed using non-linear regression as implemented in MATLAB. The t is reasonable in all cases, especially considering there is only one degree of freedom, P_s. From these plots it is possible to obtain P_s as a function of σ^{-1} and this was found to be given by:

$$P_s = P_{\max}\left\{1 - \exp\left[-k\left(\sigma^{-1} - 1\right)\right]\right\} \quad (29)$$

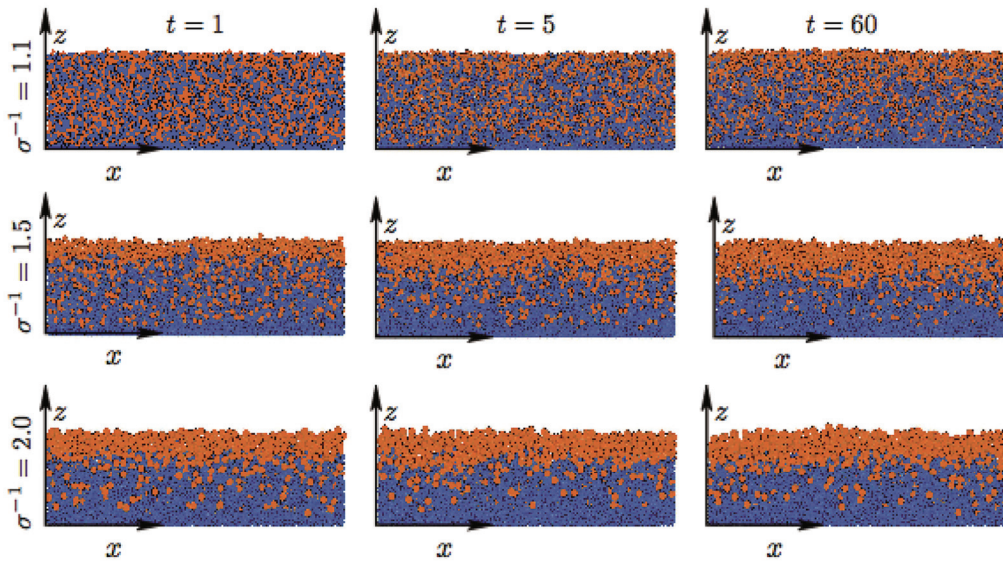where $k = 5.21$ is the saturation constant and $P_{\max} = 7.35$.

Fig. 7. *A series of snapshots from the DPM simulations with large (orange) and small (blue) particles. The rows correspond to distinct particle sizes and columns to different times. Along the top row $\sigma^{-1} = 1.1$, middle row $\sigma^{-1} = 1.5$ and bottom row $\sigma^{-1} = 2$; whereas, the left column is for $t = 1$, middle $t = 5$ and right $t = 60$.*
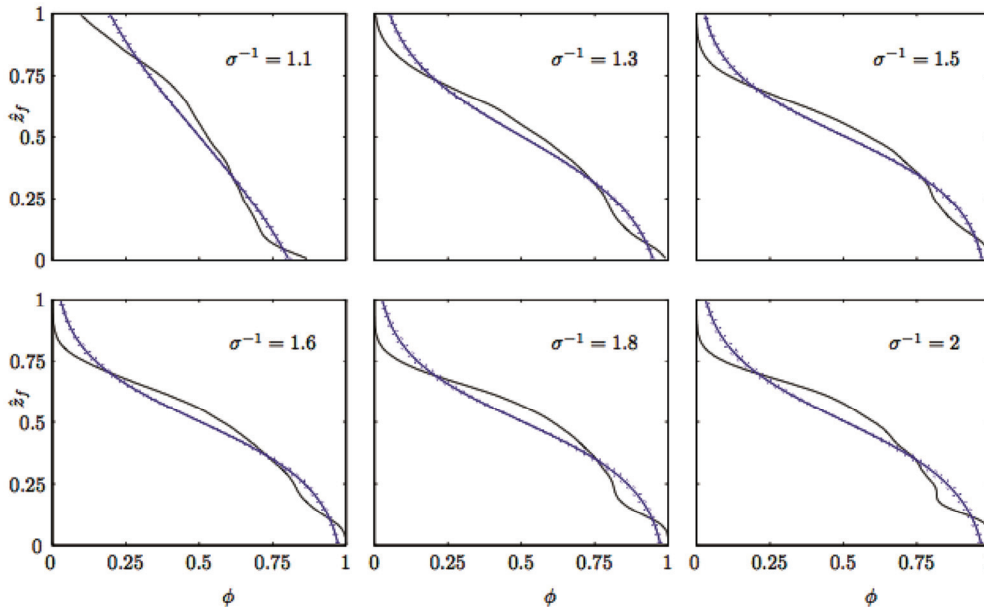

Fig. 8. *Plots of the small particle volume fraction ϕ as a function of the scaled depth $\hat{z}_f$. The black lines are the coarse-grained DPM simulation data and the blue lines are the fit to equation (28) produced with MATLAB's non-linear regression function. For the fit only P_s is used as a free parameter. Dotted lines shows the 95% confidence intervals for the fit.*

6.3. Future directions

For the segregation case the micro-macro transition has been shown to be useful in establishing the relations between the parameters that appear in the continuum descriptions and the material parameters of the particles. Additionally, in this case, we highlighted a discrepancy between the particles simulations and theory, see figure 8, i.e. the inflection point near the base in the simulation concentration profiles. Further analysis of the simulation data has shown that this discrepancy arises because the particle diffusion is not constant with depth, as assumed

by the model. Therefore, for this situation the model has to be improved to capture the full dynamics in these situations.

From a modeling point of view one of the open-topic at the moment is the determination of segregation shallow-water models, see e.g. (Woodhouse, 2012), but this is beyond the scope of this review.

7. CONCLUSIONS AND FUTURE PERSPECTIVE

Here, we have shown that continuum parameters such as the macroscopic friction can be accurately

extracted from particle simulations. We have shown that the micro-macro transition can be achieved using small particle simulations, i.e., we can determine the closure relations for a continuum model as a function of the microscopic parameters. Here, this one-way coupling from micro- to macro-variables was achieved for steady uniform flows, but can in principle be used to predict non-uniform, time-dependent flows, provided that the variations in time and space are small. Comparisons with large-scale experiments and large DPM simulations are needed to determine the range of parameters for which the steady uniform closure laws hold, as indicated in figure 1a.

However, for strongly varying flows, such as arresting flows, avalanching flows, flow near boundaries or near abrupt phase changes (dead zones, shocks), no closure relations in functional form are known. Ideally, the full 3D granular flow rheology could be determined in the full parameter space and then introduced into a pure continuum solver. However, since the parameter space is just too wide and situations can and will occur that are not covered by a systematic parameter study, other strategies and approaches can be thought of. For such interesting situations, where the rheology enters unknown regimes, or where changes are too strong and/or fast, a two-way coupling to a particle solver is a valid approach. If these complex regions are small, one can use a two-way boundary coupling, where a particle solver is used in the complex region and a continuum solver in the remaining domain, with an overlapping region where both solvers are used and where the two methods are coupled by using suitable boundary conditions (Markesteijn, 2011).

Alternatively, if the complex regions are too large to be solved by particle simulations, one can use a continuum solver where a small particle simulation is run each time the closure relations need to be evaluated (Weinan et al., 2007). This particle simulation is two-way coupled to the continuum solution in the sense that it has to satisfy the parameters set by the continuum solution (such as height, depth-averaged velocity and depth-averaged velocity gradient and boundary conditions) and return the closure relations (such as friction and velocity shape factor). Both alternative strategies provide plenty of unsolved challenges in communicating between discrete and continuous "worlds" concerning nomenclature, parameters, boundary conditions and their respective control.

The next versions of both the in-house continuum solver hpGEM (van der Vegt et al.) DPM code Mercury (Thornton et al.), are designed such that they can be easily coupled and hence used to form the basis of a granular two-way coupled code.

REFERENCES

Allen, M.P., Tildesley, D.J., 1989, *Computer simulations of liquids*, Clarendon Press, Oxford.

Babic, B., 1997, Average balance equations for granular materials, *Int. J. Eng. Science*, 35 (5), 523-548.

Bokhove, O., Thornton, A.R., 2012, Shallow granular flows, in: Fernando, H.J., ed., *Handbook of environmental fluid dynamics*, CRC Press.

Cui, X., Gray, J.M.N.T., Johannesson, T., 2007, Deflecting dams and the formation of oblique shocks in snow avalanches at flateyri, *JGR*, 112.

Cundall, P.A., Strack, O.D.L., 1979, A discrete numerical model for granular assemblies, *Geotechnique*, 29, 47-65.

Dalbey, K., Patra, A.K., Pitman, E.B., Bursik, M.I., Sheridan, M.F., 2008, Input uncertainty propagation methods and hazard mapping of geophysical mass flows, *J. Geophys. Res.*, 113.

Denlinger, R.P. Iverson, R.M., 2001, Flow of variably fluidized granular masses across three-dimensional terrain, 2. numerical predictions and experimental tests, *J. Geophys Res.*, 106 (B1), 533-566.

Dolgunin, V.N., Ukolov, A.A., 1995, Segregation modelling of particle rapid gravity flow, *Powder Tech.*, 83 (2), 95-103.

Drahun, J.A., Bridgewater, J., 1983, The mechanisms of free surface segregation, *Powder Tech.*, 36, 39-53.

Ericson, C., 2004, *Real-time collision detection* (The Morgan Kaufmann Series in Interactive 3-D Technology), Morgan Kaufmann Publishers Inc., San Francisco.

Form, W., Ito, N., Kohring, G.A., 1993, Vectorized and parallelized algorithms for multi-million particle MD-simulation, *International Journal of Modern Physics C*, 4(6), 1085-1101.

GDR Midi, 2004, On dense granular flows, *Eur. Phys. J.E.*, 14, 341-365.

de Gennes, P.G., 2008, From rice to snow, in: *Nishina Memorial Lectures*, vol. 746 of Lecture Notes in Physics, Springer, Berlin/Heidelberg, 297-318.

Gilbert, L.E., Ertas, D., Grest, G.S., Halsey, D., Levine, T.C., Plimpton, S.J., 2001, Granular flow down an inclined plane: Bagnold scaling and rheology, *Phys. Rev. E.*, 64 (051302).

Goldhirsch, I., 2010, Stress, stress asymmetry and couple stress: from discrete particles to continuous fields, *Granular Matter*, 12 (3), 239-252.

Gray, J.M.N.T., Ancey, C., 2011, Multi-component particle-size segregation in shallow granular avalanches, *J. Fluid Mech.*, 678, 535-588.

Gray, J.M.N.T., Chugunov, V.A., 2006 Particle-size segregation and diffusive remixing in shallow granular avalanches, *J. Fluid Mech.*, 569, 365-398.

Gray, J.M.N.T., Cui, X., 2007, Weak, strong and detached oblique shocks in gravity driven granular free-surface flows, *J. Fluid Mech.*, 579, 113-136.

Gray, J.M.N.T., Tai, Y.C., Noelle, S., 2003, Shock waves, dead zones and particle-free regions in rapid granular free-surface flows, *J. Fluid Mech.*, 491, 161-181.

Gray, J.M.N.T., Thornton, A.R., 2005, A theory for particle size segregation in shallow granular free-surface flows, *Proc. Royal Soc. A*, 461,1447-1473.

Hakonardottir, K.M., Hogg, A.J., 2005, Oblique shocks in rapid granular flows, *Phys. Fluids*.

Hockney, R.W., Eastwood, J.W., 1981, *Computer simulation using particles*, McGraw- Hill, New York.

Hungr, O., Morgenstern, N.R., 1984, Experiments on the flow behaviour of granular materials at high velocity in an open channel, *Geotechnique*, 34 (3).

Irwing, J.H., Kirkwood, J.G., 1950, The statistical mechanical theory of transport processes, iv. the equations of hydro-dynamics, *The Journal of Chemical Physics*.

Iverson, R.M., 2003, The debris-flow rheology myth, in: Rickenmann and Chen, eds, *Debrisow hazards havards mitigation: Mechanics, prediction and assessment*, Millpress, 303-314.

Iwai, T., Hong, C.W., Greil, P., 1999, Fast particle pair detection algorithms for particle Simulations, Int. J. Modern Physics C, 10(5), 823-837.

Jenkins, J.T., Savage, S.B., 1983, A theory for the rapid flow of identical, smooth, nearly elastic, spherical particles, *Journal Fluid. Mech.*, 130, 187-202.

Luding, S., 2004, Micro-macro models for anisotropic granular media, in: Vermeer, P.A., Ehlers, W., Herrmann, H.J. Ramm, E., eds, *Micro-macro models for anisotropic granular media*, Balkema A.A., Leiden, 195-206.

Luding, S., 2008, Cohesive, frictional powders: contact models for tension, *Granular Matter*, 10 (4), 235-246.

Luding, S., Laetzel, M., Volk, W., Diebels, S., Hermann, H.J., 2001, From discrete element simulations to a continuum model, *Comp. Meth. Appl. Mech. Engng.*, 191, 21-28.

Lun, C.K.K., Savage, S.B., Jeffrey, D.J., Chepurniy, N., 1984, Kinetic theories for granular flow: inelastic particles in couette flow and slightly inelastic particles in a general flow field, J. Fluid Mech, 140, 223.

Markesteijn, A.P., 2011, *Connecting molecular dynamics and computational fluid dynamics*, Ph.D. Thesis, University of Delft.

Middleton, G.V., 1970, Experimental studies related to problems of flysch sedimentation, in: Lajoie, J., ed., *Flysch Sedimentology in North America*, Business and Economics Science Ltd, Toronto, 253-272.

Moore, M., Wilhelms, J., 1988, Collision detection and response for computer animation, *Computer Graphics* (SIGGRAPH '88 Proceedings), 22 (4), 289-298.

Munjiza, A., 2004, *The combined finite-discrete element method*, John Wiley & Sons Ltd.

Muth, B., Mueller, M.K., Eberhard, P., Luding, S., 2007, Collision detection and administration for many colliding bodies, *Proc. DEM07*, 1-18.

Ogarko, V., Luding, S., 2010, Data structures and algorithms for contact detection in numerical simulation of discrete particle systems, *Proc. 6th Word Congress on Particle Technology WCPT6*, Nuremberg.

Ogarko, V., Luding, S., 2011, A study on the influence of the particle packing fraction on the performance of a multi-level contact detection algorithm, in: Onate, E., Owen, D.R.J., eds, *II Int. Conf. on Particle-based Methods - Fundamentals and Applications, PARTICLES 2011*, Barcelona, Spain, 1-7.

Ogarko, V., Luding, S., 2012, A fast multilevel algorithm for contact detection of arbitrarily polydisperse objects, *Computer Physics Communications*, 183 (4), 931-936.

Pesch, L., Bell, A., Sollie, W.E.H., Ambati, V.R., Bokhove, O., Vegt, J.J.W., 2007, hpgem a software framework for discontinous galerkin finite element methods, *ACM Transactions on Mathematical Software*, 33 (4).

Pouliquen, O., 1999, Scaling laws in granular flows down rough inclined planes, *Phys. Fluids*, 11 (3), 542-548.

Pouliquen, O., Forterre, Y., 2002, Friction law for dense granular flows: application to the motion of a mass down a rough inlined plane, *J. Fluid Mech.*, 453, 131-151.

Raschdorf, S., Kolonko, M., 2011, A comparison of data structures for the simulation of polydisperse particle packings, *Int. J. Num. Meth. Eng.*, 85, 625-639.

Savage, S.B., Hutter, K., 1989, The motion of a finite mass of material down a rough incline, *Journal Fluid. Mech.*, 199, 177-215.

Savage, S.B., Lun, C K.K., 1988, Particle size segregation in inclined chute flow of dry cohesionless granular material, *J. Fluid Mech.*, 189, 311-335.

Schofield, P., Henderson, J.R., 1982, Statistical mechanics of inhomogenous fluids, *Proc. R. Soc.*, 379, 231-246.

Shen, S., Atluri, S.N., 2004, Atomic-level stress calculation and continuum molecular system equivalence, *CMES*, 6 (1), 91-104.

Shinbrot, T., Alexander, A., Muzzio, F.J., 1999, Spontaneous chaotic granular mixing, *Nature*, 397 (6721), 675-678.

Stadler, J., Mikulla, R., Trebin, H.R., 1997, IMD: A software package for molecular dynamics studies on parallel computers, *Int. J. Modern Physics C*, 8 (5), 1131-1140.

Thatcher, U., 2000, Loose octrees, in: deLoura, M., ed., Charles River Media.

Thornton, A.R, Weinhart, T., Krijgsman, D., Luding, S., Bokhove, O., Mercury md. http://www2.msm.ctw.utwente.nl/athornton/MD/.

Thornton, A.R, Gray, J.M.N.T., Hogg, A.J., 2006, A three phase model of segregation in shallow granular free-surface flows, *J. Fluid Mech.*, 550, 1-25.

Thornton, A.R, Weinhart, T., Luding, S., Bokhove, O., 2012, Modelling of particle size segregation: Calibration using

the discrete particle method. Submitted to *Int. J. Mod. Phys. C.*, 23(8), 1240014.

Thornton, A.R, Weinhart, T., Luding, S., Bokhove, O., 2013, Friction dependence of shallow granular flows from discrete particle simulations. Submitted to *Eurp. Phys. Letts*.

Todd, D.,B., Evans, D.J., Daivis, P.J., 1995, Pressure tensor for inhomogeneous fluids, *Phys. Rev. E*, 52(2).

van der Vegt, J.J.W., Thornton, A.R., Bokhove, O., hpgem. http://www2.msm.ctw.utwente.nl/athornton/hpGEM/.

Vreman, A.W., Al-Tarazi, M., Kuipers, A.M., van Sint Annaland, M., Bokhove, O., 2007, Supercritical shallow granular flow through a contraction: experiment, theory and simulation, *JFM*, 578, 233-269.

Walton, O.R., Braun, R.L., 1986, Viscosity, granular temperature, and stress calculations for shearing assemblies of inelastic, frictional disks, *Journal of Rheology*, 30 (949).

Weinan, E., Engquist, B., Li, X., Ren, W., Vanden-Eijnden, E., 2007, Heterogeneous multiscale methods: a review, *Communications in Computational Physics*, 2 (3), 367-450.

Weinhart, T., Thornton, A.R., Luding, S., Bokhove, O., 2012a, Closure relations for shallow granular flows from particle simulations, *Granular Matter*, 14, 531-552.

Weinhart, T., Thornton, A.R., Luding, S., Bokhove, O., 2012b, From discrete particles to continuum fields near a boundary, *Granular Matter*, 14, 289-294.

Williams, J.R., O'Connor, R., 1999, Discrete element simulation and the contact problem, *Archives of Computational Methods in Engineering*, 6 (4), 279-304.

Williams, J.R., Stinton, A.J., Sheridan, M.F., 2008, Evaluation of the Titan 2D two-phase flow model using an actual event: Case study of the vazcun valley lahar, *Journal of Volcanology and Geothermal Research*, 177, 760-766.

Woodhouse, M., Thornton, A.R., Johnson, C., Kokelaar, P., Gray, J.N.M.T., 2012, Segregation induced fingering instabilities in granular avalanches, *JFM*, 709, 543-580.

WIELOSKALOWE METODY DLA WIELOSKŁADNIKOWYCH MATERIAŁÓW ZIARNISTYCH

Streszczenie

W artykule przedstawiono postęp w zrozumieniu przepływu przesypywanych materiałów ziarnistych, jaki został ostatnio osiągnięty dzięki technikom modelowania wieloskalowego. Na początku omówiono metodę dyskretnych cząstek (ang. Discrete particle method - DPM) i wyjaśniono w jaki sposób należy konstruować ciągłe pole na podstawie dyskretnych danych tak, aby model był spójny z makroskopową zasadą zachowania masy i pędu. Zaprezentowano też nową metodę wykrywania kontaktu, która może być wykorzystana do wieloskładnikowych materiałów sypkich o rozmiarze cząstek zmieniających się w zakresie rzędów wielkości. Pokazano jak zaawansowane symulacje DPM mogą być zastosowane do uzyskiwania zależności dla modelu ciągłego (mapowanie zmiennych i funkcji między skalami mikro i makro). To umożliwiło rozwój modeli kontinuum zawierających informację o mikrostrukturze materiałów sypkich bez potrzeby robienia dodatkowych założeń.

Przejście mikro-makro przedstawiono dla dwóch problemów płynięcia materiału sypkiego. Pierwszym jest płynięcie w płytkim zsypie, gdzie główną niewiadomą w modelu kontinuum jest makro współczynnik tarcia. W pracy badano jak ten współczynnik zależy od własności przepływających cząstek i powierzchni, względem której cząstki przepływają. Drugim analizowanym problemem jest segregacja przy zsypie polidyspersyjnych cząstek. W obydwu analizowanych problemach rozważono krótkie okresy stacjonarne w symulacji DPM, aby otrzymać realistyczne, wzajemnie dopełniające się zależności opisujące ciągłe własności materiału.

W pracy omówiono również problem dokładności i poprawności opisanych wzajemnie dopełniających się zależności dla złożonych problemów dynamicznych. Problemy te są odległe od omówionych wcześniej rozwiązań dla krótkich okresów stacjonarnych, dla których te zależności były otrzymywane. Dla prostych przypadków zastosowanie zdefiniowanych wzajemnie dopełniających się zależności dawało poprawne wyniki. W bardziej skomplikowanych sytuacjach potrzebne są nowe, bardziej zaawansowane rozwiązania, w których makrokontinuum i mikro dyskretny model są połączone w sposób dynamiczny ze sprzężeniem zwrotnym.